Two Dimensional Hybrid Model of a Miniaturized Cylindrical Hall Thruster

IEPC-2007-157

Presented at the 30th International Electric Propulsion Conference, Florence, Italy
September 17-20, 2007

L. Garrigues*, G. J. M. Hagelaar†, J. P. Boeuf‡
LAPLACE, CNRS-Université Paul Sabatier, 31062 Toulouse, France

Y. Raitses §, A. Smirnov**, and N. J. Fisch††
Princeton Plasma Physics Laboratory, Princeton University, Princeton, NJ, 08543

We use a two-dimensional hybrid model to study a miniaturized cylindrical Hall thruster (100 W of power level). The channel of thruster is constituted with a short coaxial part and a longer cylindrical region, to prevent erosion. The two-dimensional model combines a fluid description of the electrons (combining continuity with momentum equations) and a particle description of the ions and the neutral atoms. We assume a quasineutral plasma. Results show that the in order to reproduce the measured current, the anomalous transport is governed by a Bohm diffusion, with an equivalent collision frequency $\nu_B \sim \omega_c/16$ – ω_c being the cyclotron pulsation. Two-dimensional results exhibit a potential drop covering the region of large magnetic field, beginning in the coaxial part and extending until the plume region. The ionization takes place in the annular region. The origin of the high propellant efficiency, observed experimentally has been carefully studied and can be attributed to double charged ions. The low energy ions impacting on the ceramics of the cylindrical part seems not to erode the walls of the annular region.

Nomenclature

B, B_0	=	magnetic field, reference magnetic field
e	=	electron charge constant
$F_{//}$	=	magnetic field parallel force
I_{back}, I_{front}	=	back, front coil current
I_d, I_i	=	discharge, ion current
k_B	=	Bohm fitting parameter
m_a	=	xenon anode mass flow
m_e, M	=	electron, neutral atom mass
n, n_0,n_e, n_i	=	plasma, reference, electron, ion density
N	=	neutral gas density
S	=	ionisation source term

* Scientist at CNRS, LAPLACE, Toulouse, France, laurent.garrigues@laplace.univ-tlse.fr.
† Scientist at CNRS, LAPLACE, Toulouse, France, gerjan.hagelaar@laplace.univ-tlse.fr.
‡ Senior Scientist at CNRS, LAPLACE, Toulouse, France, jpb@laplace.univ-tlse.fr.
§ Research Physicist, PPPL, Princeton, yraitses@pppl.gov.
** Research Physicist, Tri Alpha Energy Inc., Foothill Ranch, CA, 92610, asmirnov@trialphanenergy.com.
†† Professor, Princeton University and PPPL, Princeton, fisch@princeton.edu.

T = thrust
T_e = electron temperature
U = fitting parameter
$v_\perp$ = electron velocity perpendicular to the magnetic field
V = electric potential
V_c, V_d = cathode potential, discharge voltage
W = electron-wall effective energy loss coefficient
x, r = axial, radial coordinate
Xe^+, Xe^{2+} = single, double charged ion
α_e = adjustable parameter
β = Boltzmann factor
ε = electron mean energy
Γ_e , Γ_i = electron, ion flux
κ = inelastic effective energy loss coefficients
$\overline{\mu}$ = electron mobility tensor
ν_B = equivalent Bohm collision frequency
ν_m = electron-atom momentum transfer frequency
η_c, η_u = current utilization, propellant utilization efficiency
θ_b = beam divergence
ω_c = cyclotron pulsation
Ω = Hall parameter
χ = magnetic moment

I. Introduction

Hall Effect Thrusters (HETs) in the range of few kW are now mature enough to be on board geostationary satellites for station-keeping missions. Efforts continue in the direction of higher electric power in to order to scale-up HETs for orbit transfer and repositioning. A scale-down of HETs operating at a lower electric power is suitable for low mass spacecraft or multiple micro-spacecraft flying in constellations for scientific missions[1].

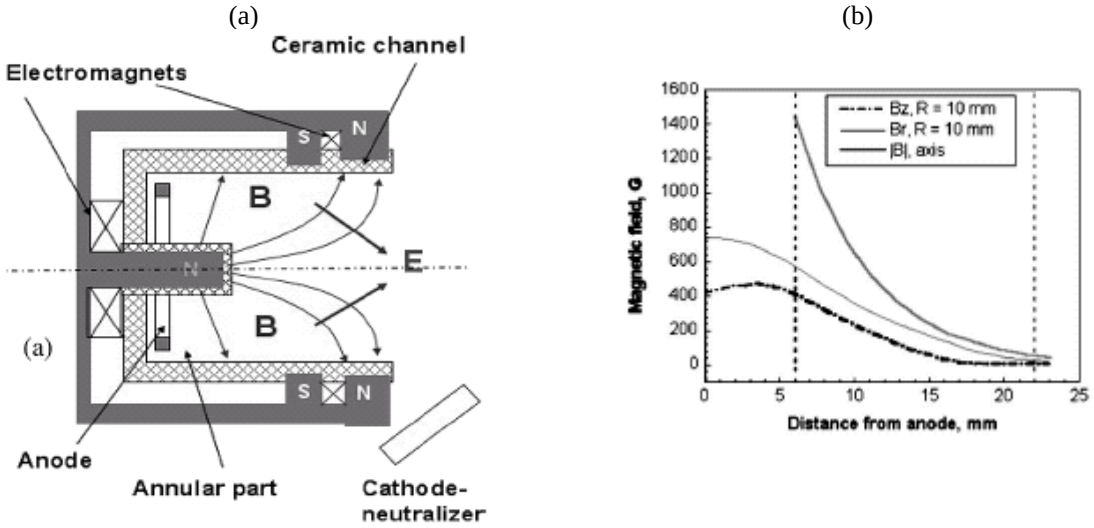

Figure 1 : (a) Schematic of the Cylindrical Hall Thruster (from Ref. 3), (b) magnetic field profiles in the MCHT, I_{back}=2.5 A, I_{front}=-1A, dashed lines at x= 6 mm and x = 22 mm show the edge of the annular channel part and thruster exit respectively (Ref. 4).

A low electric power available on small satellites implies either a low applied voltage either a low discharge current. To maintain a high specific impulse, the ions must be accelerated at high velocities. As a result, a reduce of electric power implies a decrease in the discharge current. The consequence is that a low neutral mass flow must be injected. To maintain a high ionisation efficiency (which means a large ionisation of the injected mass flow) in a lower channel length, the magnetic field must be increased. The magnetic saturation of the circuit near the inner pole induces challenges to reach an optimal magnetic field magnitude. Moreover, because there is no room for an inner coil, a scale down of the thruster size leads also to some difficulty to achieve a desired magnetic field shape. The magnetic field in the exhaust region can not be radial, leading to large ion losses and inner wall erosion. Low power HETs, based on conventional annular channel, operating in the range of 100-300 W offer low efficiency[2].

Another concept of electromagnetic thruster based on axial electric field and radial magnetic field as in a HET has been proposed few years ago. This concept named Cylindrical Hall Thruster (CHT) (see Ref. 3) features a channel with a short annular region and a longer cylindrical region as in Figure 1. The xenon mass flow is injected through the anode, the ceramics of the channel are made in boron-nitride as in conventional HETs. Two coils (a front and a back one) are connected to separate power supply. A cusp magnetic field shape is obtained with counterdirected coil currents, as shown in Figure 1. Compared to conventional annular geometry, the CHT offers a lower surface-to-volume ratio, and, potentially, smaller ion losses and wall erosion of the inner part[4]. A new concept of CHT has been proposed with a configuration without a short coaxial region, which can be a benefice for the thruster lifetime[5].

The Miniaturized CHT of 2.6 cm diameter (MCHT) has been characterized first in the Princeton Plasma Physics Laboratory (PPPL) Small Hall Thruster facility. The working gas pressure of xenon was about 7×10^{-5} Torr for a total propellant mass flow of 0.8 mg/s[6]. The current-voltage characteristics and the MCHT performance (thrust, efficiency, etc.) have been measured for discharge voltages between 150 and 300 V, and xenon mass flow at the anode in the range 0.4 – 0.8 mg/s. The plasma potential, ion density and electron temperature have then been measured inside the MCHT by means of stationary and movable floating emissive and biased Langmuir probe[7]. Plume diagnostics (planar probe and two-grid retarding potential analyser) able to rotate +/- 90° from the thruster axis positioned at 72 cm from the channel exit have permit to measure the ion flux angular distribution and the ion energy distribution function in the plume[8]. In parallel to the experimental studies, theoretical approach has been carried out in order to understand the electron cross-field transport in such complex magnetic field topology[9].

The main conclusions of these experimental and theoretical studies can be summarized as the following :

(i) the propellant utilization (being defined as the ratio of ion current considering single-charged ions to the propellant mass flow expressed in units of electric current) in the MCHT is higher than a conventional annular HET of same diameter. Moreover, the propellant utilization in the MCHT is higher than one, a significant fraction of double-charged ions seems to be present ;

(ii) the plasma density is non uniform in the radial direction with the peak at the thruster axis, the potential drop is concentrated mainly in the cylindrical part of the channel and in the plume, the ion bombardment on the ceramic walls should be reduced in comparison with annular HET. The role of the diamagnetic force has been advanced as hypothesis to understand the axial gradient of electric potential;

(iii) the ion beam divergence, defined as the angle which contains 90% of the ion current, is large 70-80° (compared to 45° for standard HETs) which of course leads to a thrust reduction in the axial direction. A segmented electrode is used (with a positive bias of 50-100 V with respect to the cathode) to initiate a precursor discharge between this electrode and the cathode (few watts are necessary), the main discharge between the thruster anode and the cathode is easily initiate, and the ion beam divergence MCHT is then reduced to 55° ;

(iv) the electron transport in the direction perpendicular to the magnetic field lines is governed by Bohm type anomalous diffusion with a collision frequency ν_B on the order of the Bohm value ($\nu_B \sim \omega_c/16$ – ω_c is the cyclotron pulsation).

A two-dimensional model has been developed in the context of conventional HETs[10] and extended to Double-Stage Hall Effect Thruster[11]. This model assumes a quasineutral plasma. The plasma density profile is deduced from the ion kinetic approach, trajectories of a large number of ions created according to a source term are followed until the macro-ions leave the domain or impact on ceramic walls. Neutral particles are injected in the simulation domain through the anode plane and ionised by high electron energies. We use a fluid description to describe the electron transport, taking into account some anomalous transport. The electric potential is not deduced from a Poisson equation but from a Ohm's law. We present in this paper the calculations of electric potential without assuming a Boltzmann equilibrium but we solve a two-dimensional elliptic equation to calculate the electric potential profile[12].

We also account for diamagnetic force (also called mirror force). The goal of this paper is to use the two-dimensional hybrid model to examine the MCHT operation.

The paper is organized as the following, we describe the model in section II, the results are detailed and commented in section III. We finally end this paper with a conclusion in section IV.

II. Description of the model

In the two-dimensional hybrid model, the treatment of the heavy species (ions – single and double charges and neutrals) derives from particles tracing as done in PIC simulation (see sub-section A.). The electron transport is described with fluid equations, and the electric potential profile in two-dimensions (without assuming a Boltzmann relation along the magnetic lines) taking into account the mirror force is calculated from a current conservation equation forcing quasineutrality (see sub-section B.). We end this section (see sub-section C.) with the procedure used to fit the anomalous cross-field electron conductivity and the electron wall energy losses by comparisons between calculations and experimental results.

A. Ion and neutral transport

The motion of heavy particles Xe, Xe^+ and Xe^{2+} is solve in three dimensions. The computational domain assumes a cylindrical symmetry and extends on 4.5 cm in the axial direction *x*, and 6 cm in the radial direction *r*. The domain contains the channel of the MCHT (annular and cylindrical regions) and the cathode. The cathode is positioned at r = 5.4 cm and x = 3.5 cm. We typically use 60 cells in the x direction and 80 cells in the r direction. For practical reasons, we use the macro particle technique, as in PIC model, where a weight schema decides how many ions and neutrals are represented by a macro-particle. The neutrals are injected in the anode plane assuming a Maxwellian distribution of the flux in the axial direction for a given temperature equal to 500 K. We also account for the background neutral atoms due to the backpressure tank by injecting an additional neutral flux at the thermal velocity (temperature of 300 K) from the boundaries of the computational domain in the near field region. The mass flow of neutral atoms through the cathode with a mass flow of 0.2 mg/s has also been included in some simulations (see sub-section III.B.) The effect of the neutral atoms flowing through the cathode orifice has been considered assuming that the temperature of neutral atoms are in equilibrium with the walls (a rough estimation gives a temperature ~ 1200 K[13]). Neutrals colliding with the walls are reflected back in the domain. We calculate the neutral density on the node of the computational domain.

In the present study, the doubly charged ions are included and are treated as singly charged ions. The origin of Xe^{2+} is the direct double ionization of ground state of xenon and the stepwise ionization of Xe^+. We neglect the effect of triply charged ions, the ionization threshold for ground state is 70 eV for xenon. As the single charge ions, the ion source term of double charged ions is calculated assuming a maxwellian distribution function for the electrons. Due to the large Larmor radius, the magnetic field effect on the ions is neglected. The ion trajectories are followed until the xenon ions leave the computational domain or impinge the walls. When ions impact on walls, they are neutralized and new neutral atoms are re-emitted. We calculate the ion density and flux on the node of the computational domain. We put some diagnostics to calculate the ion beam properties (energy and angular distributions) and the ceramic wall erosion due to high energetic ions (for this latter the reader can refer to Ref. 14).

B. Electron transport

The electron fluid transport is described with the continuity, momentum and energy equations. The equation for the electron conservation is given by :

$$\frac{\partial n_e}{\partial t} + \nabla \cdot \mathbf{\Gamma}_e = S \qquad (1),$$

where n_e is the electron density, $\mathbf{\Gamma}_e$ is the electron flux, and S the ionisation source term.

The electron transport is currently a balance between the electric force and the kinetic pressure gradient. The complex magnetic configuration of the MCHT leads to a large magnetic field gradient along the magnetic field lines, the magnetic field magnitude B is around 1400 G at the central ceramic piece wall, and 10 G in the exhaust plane on the same magnetic field line. This mirror type structure (as in end Hall ion source – Ref. 15) near the

thruster axis leads a supplementary force which acts on the electron transport. This force is called in the literature diamagnetic force or gradB force or mirror force. In conventional HETs, this force does not play a major role.

Let us consider an individual electron of mass m_e moving along a given magnetic field line, in absence of collisions and if thee variation of the magnitude of magnetic field is small during the cyclotron rotation (adiabatic approximation), the magnetic moment χ is conserved :

$$\chi = \frac{m_e \mathrm{v}_\perp^{\,2}}{2B} = cons\tan t \tag{2},$$

where we note the perpendicular velocity of the electron $\mathrm{v}_\perp$. A parallel force appears which transforms the perpendicular (parallel) velocity in a parallel (perpendicular) velocity which pushes the electron against the magnetic field gradient :

$$F_{//} = -\chi \nabla_{//} B = -\frac{m_e \mathrm{v}_\perp^{\,2}}{2B} \nabla_{//} B \tag{3}.$$

If we now consider a Maxwellian distribution of electrons :

$$< F_{//} >= -\frac{m_e < \mathrm{v}_\perp^{\,2} >}{2B} \nabla_{//} B = -eT_e \frac{\nabla_{//} B}{B} \tag{4},$$

where e is the electron charge constant and T_e is the electron temperature. When the diamagnetic force is included, the electron momentum equation is then written – in the form of drift-diffusion approximation – as :

$$\mathbf{\Gamma}_e = \overline{\mu}\left(n_e \nabla V - \nabla\left(n_e T_e\right) - n_e T_e \frac{\nabla B}{B}\right) \tag{5}.$$

We recognize the electric force and the kinetic pressure gradient in the first and second term of eq. (5) respectively. Due to the magnetic field, the mobility $\overline{\mu}$ is not a scalar but a tensor[16], where the component of parallel and perpendicular to the magnetic field are given by the following relations :

$$\mu_{//} = \frac{e}{m_e \nu} \tag{6},$$

$$\mu_\perp = \frac{1}{1+\Omega^2} \mu_{//} = \frac{e\nu / m_e}{\nu^2 + \omega_c^{\,2}} \tag{7},$$

where Ω is the Hall parameter ($\Omega = \omega_c/\nu$ - ν being the electron-neutral collisions frequency). For typical conditions, the Ω parameter varies between 10^2 and 10^4, the perpendicular mobility is therefore lower by orders of magnitude than the parallel one.

Combining eqs. (4) and (5), and forcing quasineutrality ($n \approx n_i \approx n_e$), the electric potential V is calculated solving the following equation :

$$\nabla.\mathbf{\Gamma}_e = \nabla.\left[\overline{\mu}\left(n \nabla V - \nabla\left(nT_e\right) - nT_e \frac{\nabla B}{B}\right)\right] = \nabla.\mathbf{\Gamma}_i \tag{8}.$$

In eq. (8), the plasma density n as well as the ion flux $\mathbf{\Gamma}_i$ are deduced from the ion transport.

The elliptic equation above is solved on the same computational grid than the grid used to transport ion and neutrals. The difficulty in the resolution of eq. (8) comes from the strong anisotropy of the mobility tensor $\overline{\mu}$. A

accurate numerical scheme must be used, otherwise, the cross-field transport (in the perpendicular direction) is determined by the numerical errors and not by physical cross-field transport[12].

If we assume along the magnetic field line an equilibrium between the field force and the pressure gradient, eq. (5) becomes :

$$n\nabla_{//}V - nT_e\frac{\nabla_{//}B}{B} \approx \nabla_{//}\left(nT_e\right) \tag{9},$$

if we assume a constant electron temperature along the magnetic field lines, we obtain the well-known Morozov relation which account for the diamagnetic force[17] :

$$V = V^* + T_e \ln\left(\frac{n}{n_0}\right) + T_e \ln\left(\frac{B}{B_0}\right) \tag{10},$$

where V^* is constant along the magnetic field lines, the subscripts 0 denotes reference values.

The Boundary conditions are fixed potential at the cathode V_c=0 and at the anode V_c=V_d – where V_d is the discharge voltage. We impose on the dielectric walls, on the front plane and on the open frontier of the computational domain (near field plume region) an equality between the electron flux $\mathbf{\Gamma}_e$ and the ion flux $\mathbf{\Gamma}_i$.

In order to determine the electron temperature T_e (or the electron mean energy ε=3/2βT_e - β is the Boltzmann factor), we solve an energy equation :

$$\frac{\partial(n\varepsilon)}{\partial t}+\frac{5}{3}\nabla\cdot(\mathbf{\Gamma}_e\varepsilon)-\frac{10}{9e}\nabla\cdot(\mu n\varepsilon\nabla\varepsilon)=e\mathbf{\Gamma}_e.\nabla V-Nn\kappa-nW \tag{11},$$

N being the neutral gas density. The last two terms in the energy equation represent energy loss by collisions with gas particles and with the walls, respectively, where κ and W are effective energy loss coefficients. The inelastic rates between electrons and neutrals are calculated assuming a Maxwellian distribution and given set of cross sections. The inelastic cross sections (single direct ionisation and excitation) come from Puech and Mizzi[18]. The doubly direct ionisation cross sections from the xenon ground state come from Wetzel et *al.*[19] The cross section for ionisation of Xe^+ are deduced from Ref. 20.

C. Cross field electron mobility and electron-wall energy losses

As in conventional HETs, the electron cross-field transport still an open problem in the MCHT. A Monte Carlo model of the electron dynamic has been developed in order to quantify the mechanism responsible of the electron transport in direction perpendicular to the magnetic field[9]. The numerical domain accounts for elastic and inelastic collisions with neutrals (assuming a constant neutral density into the computational domain), electron-wall collisions (including secondary electron emission and electron attachment), and Bohm diffusion (through an equivalent collision frequency). The main conclusion of this study is that the main mechanism which can explain the cross-field transport is the Bohm diffusion $\nu_B \sim \omega_c/16$, the electron-wall interactions playing a role only on the electron energy losses.

Based on the same idea, in the hybrid model, we treat the electron cross-field transport with a frequency related to a momentum transfer between electron and neutrals (ν_m – the momentum transfer frequency is assumed constant k_m=2.5×10^{-13} m^{3}s^{-1}) and due to field fluctuations (with an equivalent frequency ν_B =$k_B\omega_c$/16 - k_B being a fitting parameter) :

$$\mu_\perp = \frac{e\nu/m_e}{\nu^2+\omega_c{}^2} \approx \frac{m_e\nu}{eB^2} = \frac{m_e\left(\nu_m+\nu_B\right)}{eB^2} \tag{12}.$$

In order to quantify the k_B parameter, we have calculated the discharge current I_d and the current utilization efficiency η_c defined as I_i/I_d as a function of k_B. For a discharge voltage of 250 V and a mass flow rate of 0.4 mg/s, experiments have been investigated in the EPPDyL facility to measure the discharge current and the current

utilization efficiency. Simulated values of I_d and η_c give a better agreement for k_B=1 (see fig. 2), confirming a k_B parameter few times larger than those of conventional HETs[21] ($k_B \sim 0.1 - 0.2$). The level of field fluctuations seems higher in the MCHT, but the hybrid model is not able to explain why. Nevertheless, we can remark that the magnetic field reaches 700 G in the annular region, 3 or 4 times higher than the magnetic field magnitude in the exhaust plane of a conventional HET. The cross-field transport must be increased in the same ratio in order to explain the measured discharge current. We have postulated that the k_B parameter can keep constant when the discharge voltage varies (see section III.).

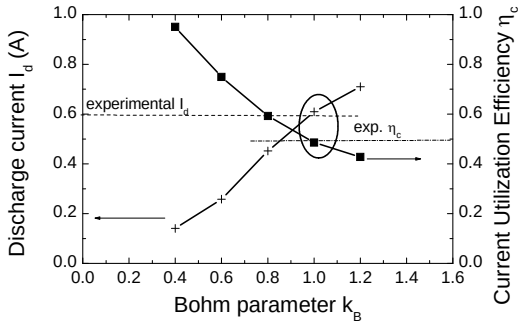

Figure 2 : Calculations of the discharge current I_d and current utilization efficiency η_c for different values of the k_B coefficient. The conditions are the following : a discharge voltage V_d of 250 V, a mass flow of xenon of 0.4 mg/s, and a facility backpressure of 9 mPa.

The fluid model shows that energy losses due to electron-atom collisions are not sufficient to reproduce experimental results. To represent energy losses due to electron-wall interactions, we use in the present paper the same empirical energy loss coefficient as in Ref. 10. The energy loss per second per electron is taken as :

$$W = \alpha_\varepsilon 10^7 \varepsilon \exp\left(-\frac{U}{\varepsilon}\right) \quad (13),$$

where α_ε and U are constant fitting parameters. We have compared the calculated and the measured electron mean energy ($\varepsilon = 3/2 k_B T_e$) to fix the α_ε and U parameters. Figure 3 shows an acceptable agreement between the measured and the calculated profile of ε for α_ε = 0.7 and U = 20 eV (the conditions are the same than figure 2, and k_B=1). The boundary conditions are the following, we assume a given electron mean energy of 10 eV on the anode plane, 10 eV in the cathode, and 5 eV in the near plume region.

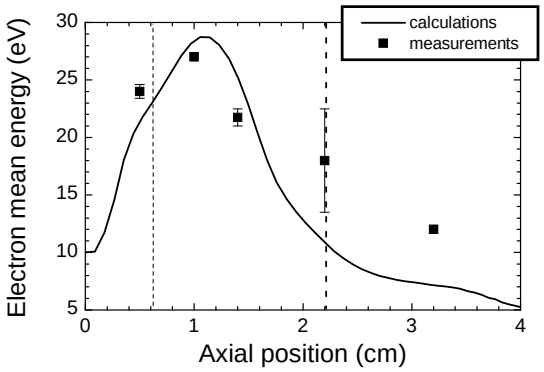

Figure 3 : Calculated and measured[7] profiles of the electron mean energy near the outer wall. The dashed lines at x = 0.6 cm and x = 2.2 cm represent the edge of the annular channel region and the thruster axis respectively. The conditions are the same than those of figure 2. The vertical bars indicate the interval in which the electron mean energy is located.

III. Results and discussion

We performed calculations for a given set of coil currents I_{back} = 2.5 A, I_{front} = -1 A, for two anode mass flow 0.4 and 0.6 mg/s, the discharge voltage varies from 200 to 300 V. We present in sub-section A. the plasma characteristics for an anode mass flow of 0.4 mg/s and a discharge voltage of 250 V, we also compare simulation results with experimental measurements of electric potential and plasma density. The current-voltage characteristic and the propellant utilization efficiency are presented in sub-section B., we analyse in the same sub-section the origin of a large propellant efficiency in the MCHT. We end this section with a study of the ion distribution function as a function of the energy and angle and the consequence of ion bombardment on the thruster lifetime (see sub-section C.)

A. Plasma characteristics

The time-average spatial distributions of electric potential, ionization source term, neutral atom and ion densities are given in Figure 4 for V_d = 250 V, for a anode xenon mass flow of 0.4 mg/s, and for a backpressure of 9 mPa. We made a zoom in the radial direction to focus on the plasma zone in the results presented fig. 4. The cathode effect through a supplementary injection of neutral atoms is not included. Fig. 4a shows the magnetic field lines and we note that the computational domain extends to a region where the axis of symmetry is taken into account. The computational domain is not now limited by the magnetic field lines which intercepts the cathode, as in previous studies where the electric potential was calculated assuming a Boltzmann relation for the electrons[10, 13, 22]. The electric potential contours shown in Fig. 4b demonstrates that the potential drop is concentrated in the region of high magnetic field which covers the annular and cylindrical parts, with a non negligible drop outside the exit plane. We also see that the electric potential contours do not follow the magnetic field lines inside the coaxial part and outside the MCHT channel. We observe that the electric potential variation along a magnetic field line which intercepts the magnetic inner pole and the cathode is few ten's of V. Numerical simulations carried out in the context of conventional annular HETs of 1.5 kW only show a potential variation of few V in the same region[22].

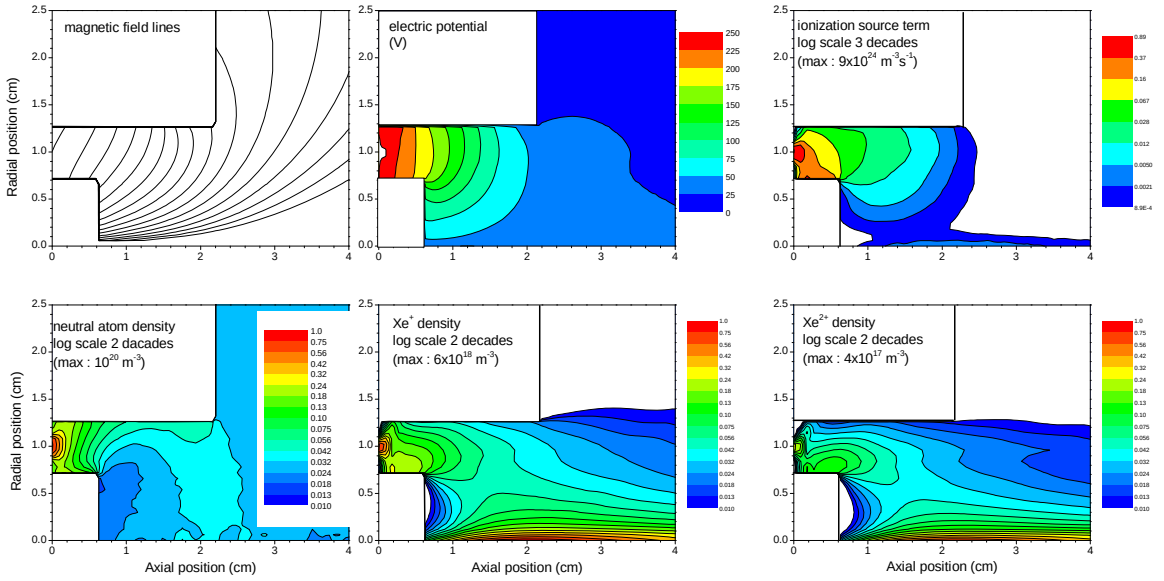

Figure 4 : Plasma characteristics for a discharge voltage V_d of 250 V, for a anode mass flow of xenon of 0.4 mg/s, and for a facility backpressure of 9 mPa.

The maximum of ionization is achieved in the annular region as we see in Fig. 4c. In this region, the neutral atom density is large (see Fig. 4d), the electron energy exceed 10 eV as we note in Fig. 3, and the electrons are largely confined by the strong magnetic field magnitude. The neutral density is maximum in front of the region of atom injection as expected (~10^{20} m^{-3}), then largely decreases due to the intense ionization. We note a region of non-negligible atom density due to ion recombination near the outer wall of the cylindrical region (see sub-section III.C.). The neutral atom density in the outside region is about 2×10^{18} m^{-3} arising from the backpressure flow. We

observe in Fig. 4e two peaks of Xe^+ ion density, the first one in the annular zone due to the ionization of the neutral gas (density in the range of 4×10^{18} m^{-3}) and the second one in the region of the axis of symmetry (~ 5×10^{18} m^{-3}) due to convergent ion flux. We also note that some ions impact in the inner wall of the annular region, the possible damage on the erosion and thruster lifetime will be examined further. Although the xenon mass flowing through the anode is relatively low (10 times less than the mass flow injected for 1 kW HETs), we have noticed an intense Xe^+ ion density due to the small channel cross-section and volume of the annular region of the MCHT (2 cm^{-3} to be compared with the 50 cm^{-3} of the 9 cm diameter CHT). A possible effect of Xe^{2+} has been invoked to a possible explanation of the high propellant efficiency of the MCHT[6]. We have reported in Fig. 4f the profile of Xe^{2+} ion density, we observe that the profile has the same shape than the Xe^+ ion density profile, which indicates that the Xe^{2+} ions are mainly produced by ionization of the single charged ions. The electron energy is not large enough to produce Xe^{2+} ions by direct impact ionization of the xenon atom. The interesting result is that the fraction of double charged ions already represents few percent of the total ion density for a anode mass flow of xenon of 0.4 mg/s. Same calculations for a mass flow of 0.6 mg/s leads to a higher density in the coaxial part with a percentage of double charged ions which attains 10 % of the total ion density.

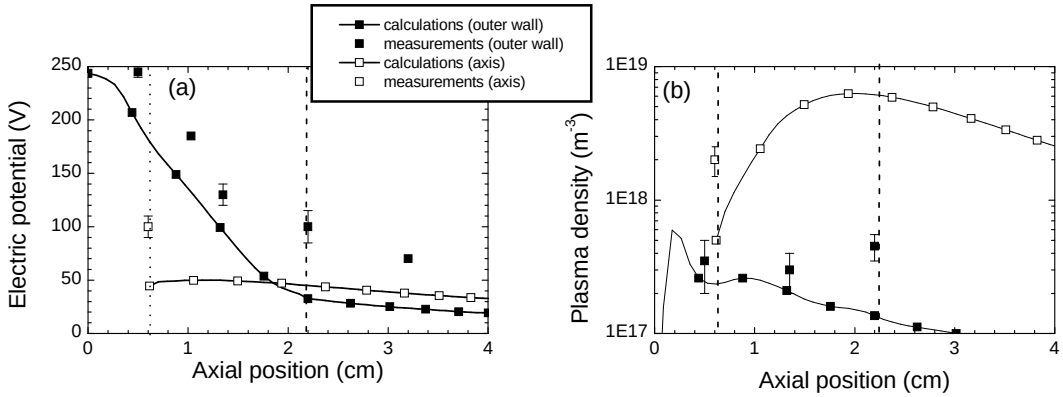

Figure 5 : Comparisons between calculated and measured profiles[7] of (a) electric potential and (b) plasma density for a discharge voltage V_d of 250 V, for a mass flow of xenon of 0.4 mg/s, and for a facility backpressure of 9 mPa. The vertical bars indicate the interval in which the measured quantities are located.

We have compared the calculated and experimental profiles of electric potential and plasma density (see figure 5). The agreement between simulated and measured values of electric potential as we observe in Fig. 5a is far from been perfect. Especially, the potential drop begins in the cylindrical region and extends beyond the exit plane in the experiments, while a non negligible potential drop inside the annular region exits in the calculations, and the calculated electric potential in the plume (beyond the exit plane) only reaches few ten's of V. The calculations confirm a large electric potential on the axis of symmetry. We can make two remarks, the first one is related to the effect of anomalous transport coefficient on the electric potential profile, as it has been shown in Refs. 21 and 22. We have taken the same anomalous Bohm coefficient in the annular and cylindrical regions, but there is no evidence to do that. A high Bohm coefficient inside the annular region guarantees a large electron conductivity leading to a smaller potential drop inside this region. The second remark concerns the diamagnetic effect, which varies linearly with the electron temperature T_e (eq. 8). We underestimate the electron energy in the region near the exhaust plane (see Fig. 3) by a factor of 2, which maybe can explain some differences between the simulated and measured values of electric potential in this region. Again, we use the same parameter to account for the electron energy losses due to electron-wall interactions inside and outside the coaxial part. The boundary condition on the electron energy in the plume also affects the simulation results.

As observed experimentally, the calculated plasma density near the outer wall is lower than in the thruster axis by more than one order of magnitude (see Fig. 5b). We note some difference beyond the exit plane, the measured plasma density reaches 6×10^{17} m^{-3}, that is 3 times the calculated plasma density at the same location. It is maybe due to the ionisation of neutrals coming from ion recombination. We observe a non negligible neutral density in the cylindrical region near the outer wall (see Fig. 4d), but it seems that the ionisation of the neutral atoms is still low, perhaps due to a low electron energy in the channel exit region.

B. Ion current and current-voltage characteristics

We have plotted in the figure 6a the discharge current as a function of the discharge voltage for two anode mass flow of xenon (0.4 and 0.6 mg/s), and for discharge voltages in the range of 200 – 300 V. The agreement between the measured and calculated current is reasonable, since the coil currents is kept constant in all the calculations.

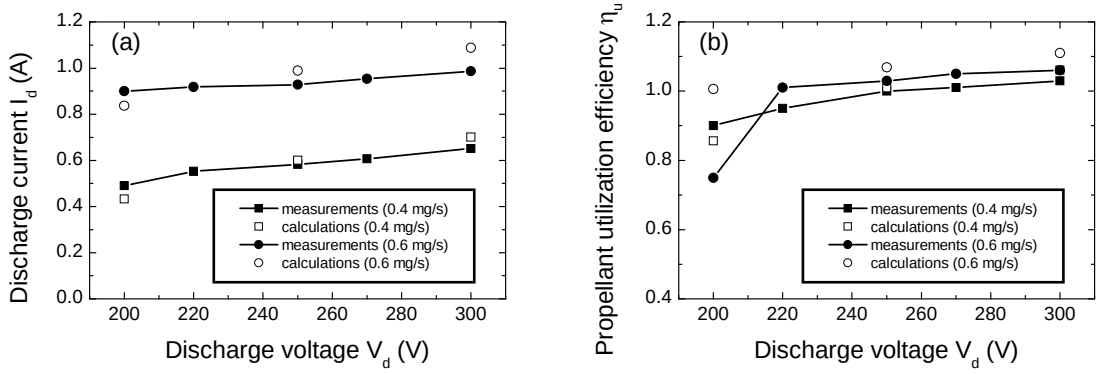

Figure 6 : (a) current-voltage characteristic for two anode mass flow of xenon, (b) propellant utilization efficiency versus discharge voltage. The facility backpressure is 9 mPa.

A more interesting result is presented in fig. 6b, where we have calculated the propellant utilization efficiency noticed η_u in the same conditions than in fig. 6a. We recall that η_u is defined as

$$\eta_u = \frac{I_i M}{e m_a} \tag{14},$$

where I_i is the total ion current, M is the mass of the propellant gas and m_a is the anode mass flow of xenon. In the definition of η_u, ion current is expressed in units mass flow considering that the ions leaving the thruster are single charged. We observe in fig. 6b that η_u is higher than 1 at high voltage. The possible mechanisms responsible for a large η_u are the presence of double charged ions and/or a residual neutral atom mass flow which can result from the neutral facility backpressure and from the neutral flowing through the cathode. We then have examined different scenarios in order to understand the origin of the high propellant utilization efficiency in the MCHT.

CASE	Facility backpressure (mPa)	xenon cathode flow (mg/s)	double charged ions	propellant efficiency η_u
1	0	0	No	0.95
2	0	0.2	No	0.95
3	9	0	No	0.96
4	20	0	No	1.00
5	30	0	No	1.15
6	0	0	Yes	1.04

Table 1 : Calculations of propellant efficiency η_u for different conditions, for a discharge voltage V_d of 250 V, for a mass flow of xenon of 0.6 mg/s.

We have fixed the anode mass flow to 0.6 mg/s and the discharge voltage to 250 V. We summarize the conditions studied and the calculated propellant efficiency η_u in Table 1. In CASE 1 we have turned off the residual neutral density induces by the facility or the cathode, and the Xe^{2+} ions are not taken into account, η_u reaches 0.95. In CASE 2, we have introduced a supplementary xenon flow through the cathode. Note that we make an assumption concerning the orientation of the cathode. For simplicity, the angle between thruster and the cathode is 90°, while in

experiments, this angle is fixed to 30°. The neutral density which results from the neutral flux flowing through the cathode orifice is then overestimated in the calculations. Nevertheless, we observe that the neutral flow cathode does not play any role. The influence of the cathode on the propellant efficiency has been recently studied experimentally, no effect has been noticed[23]. We have to remark that the negligible influence of the neutral flow through the cathode is also related to the position of the cathode. The cathode is positioned far from the channel exit, in a region of low electron energy. A cathode positioned near the channel exit in a region of large electron energy could play another role. In CASE 3, CASE 4 and CASE 5, we made a study on the sensibility of tank backpressure on η_u. We note that, in the conditions of the PPPL vacuum facility (9 mPa ~ 7×10^{-5} Torr), the propellant efficiency remains below the calculated values reported in Fig. 6b (η_u = 1.06). To reach η_u = 1.06, the backpressure must be in the range of 25 mPa. This result is not so surprising, if we think that, as we increase the anode mass flow rate (for a constant discharge voltage), the neutral density near the anode increases, the role of the neutral density induces by the backpressure is then reduced. In other words, the backpressure does affect the propellant efficiency at low xenon anode mass flow, but its influence saturates as the anode mass flow increases. Finally, in CASE 6, we have introduce Xe^{2+} ions, we not a large increase of the propellant efficiency. From this study, we can conclude that the Xe^{2+} ions seem to play a large role in the observed high propellant efficiency in the MCHT.

C. Ion distributions and wall erosion

We present the ion energy distribution function as a function of ion energy with and without the double charged ions, the distribution is maximum for a ion energy of 200 eV (for a discharge voltage of 250 V), we also distinct the fraction of double charged ions whose energies vary from 300 to 400 eV. An important issue concerns the divergence of the ion beam θ_b in the MCHT. A large beam divergence θ_b leads to a reduction in the thrust which scales as $cos\ \theta_b$. The ion beam divergence is often defined as the angle containing 90 % of the total ion current. Measurements have confirmed that the large radial electric field in the MCHT induces a half plume angle as large as 70-80° (to be compared to the 45° angle of annular HETs). Recently, the divergence has been reduced to 50° optimizing the magnetic field and using segmented electrodes[8]. We have plotted in Fig. 7b the variation of the ion beam as a function of the angle, the half plume angle is 50° in the calculations, maybe due to a lower radial electric field in the calculations. We must point out that previous calculations in the context of conventional HETs of 1 kW always underestimate the divergence of the ion beam[22]. We note that the half plume divergence does not change very much at large angle when the Xe^{2+} ions are taken into account. More work is needed concerning the magnetic field optimization and the role of segmented electrode in the MCHT in the optimization of the MCHT plume divergence.

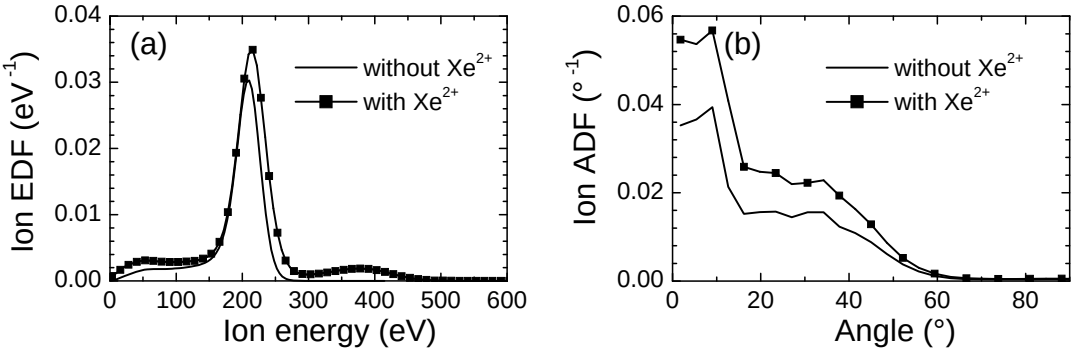

Figure 7 : Ion energy distribution function as a function of the ion energy and angle for a discharge voltage V_d of 250 V, for a mass flow of xenon of 0.6 mg/s.

A critical issue is related to the thruster lifetime, especially the possible erosion of the walls of the coaxial part. A different MCHT was recently tested by A. Shirasaki and H. Tahara[5] with a special configuration without a coaxial region. We have observed a large ionization of the neutral flow inside the annular region (see fig. 4c), the influence of ion bombardment on the thruster lifetime must be then carefully examined. The thickness of ceramic eroded as a function of the axial position is presented in fig. 8. We observe that the inner wall of the coaxial region is not eroded (less than 0.2 mm for 1000 hours of thruster working), the energy of ions impacting on walls is too low to induce a

strong erosion of the ceramic in the annular region. We note that the outer wall of the cylindrical channel in the region of exhaust suffers to a larger erosion of the ceramic (1.7 mm for 1000 hours of thruster working) because the ions impacting on the channel walls in this area have been accelerated to energy of 150 eV. This result is not in agreement with experimental observations, which suggest no visible erosion of the outer wall. The high plasma density near the center pole piece poses a question of possible erosion of the central ceramic piece. Signatures of this erosion were seen in experiments, but not in simulations. This is because the majority of the ions are accelerated in the direction opposite to the walls.

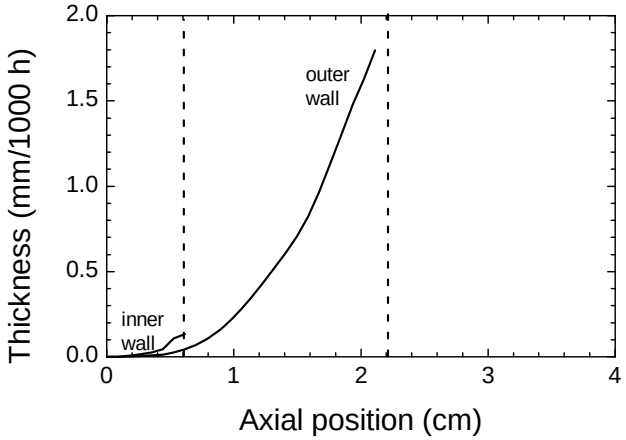

Figure 8 : Eroded thickness for a discharge voltage V_d of 250 V and for a mass flow of xenon of 0.6 mg/s.

IV. Conclusions

According to scaling low, the magnitude of the magnetic field must be increased as the dimension of the HETs is reduced in order to preserve a high degree of ionization of the neutral flux. Scaling to small sizes HETs is questionable because there is no room to position an inner coil. The optimization of the magnetic field configuration is made difficult leading to large ion wall losses and possible erosion of the thruster channel. The efficiency of conventional HETs remains low. A new thruster (MCHT) has been proposed, it combines a short coaxial part and a cylindrical region, to privilege a large volume-to-surface ratio to reduce erosion. The MCHT has been intensely studied experimentally and theoretically, nevertheless, number of questions remains open.

The aim of the study is to use a two-dimensional hybrid model in order to answer some questions or confirm some hypothesis concerning the thruster operation. We have modified the calculation of the electric potential without assuming a Boltzmann relation as previously done in simulations of HETs. We solve a two-dimensional elliptic equation combing the continuity with the momentum equations assuming a quasineutral plasma. We have taken into account the diamagnetic force (also known as mirror force) which can play a role in the magnetic field configuration of the MCHT. The double charged ions and the additional flow of neutral atoms through the cathode have taken into account in the simulations. We can summarize the main results as the following :

(1) The anomalous transport is controlled by Bohm diffusion, the equivalent collision frequency is on the order of $\nu_B \sim \omega_c/16$, as already obtained by Monte Carlo simulations of electron transport. Simulations of HETs of 10 cm size predict $\nu_B \sim \omega_c/80$. The plasma instabilities seem to play a higher role in the special magnetic field configuration of the MCHT. However, the hybrid model is not able to explain why.

(2) The potential drop begins in the annular region, sharply decreases in the cylindrical part. The electric potential in the plume is few ten's of eV. The ions are generated mainly near the anode, and we observe two peaks of plasma density, the first one in the annular region and the second one on the thruster axis due to converging ion flux. Comparisons between experimental and calculated profiles of electric potential and plasma density leads to some differences. One can argue that the constant parameters used to describe the anomalous Bohm transport and electron energy losses due to electron-wall collisions have to be refine. However, it seems that the underestimate calculation of the electron temperature near the

channel exit leads to an underestimate of the diamagnetic force and gradient of pressure near the pole piece.

(3) The calculations show a high level of propellant efficiency. Different scenarios have been proposed to understand the origin of high propellant efficiency. We have seen that the supplementary xenon cathode flow or facility backpressure do not play a crucial role. The double charged ions produced by ionization of Xe^+ highly influences the level of propellant efficiency.

(4) The ion beam divergence of 50% has been calculated, while only optimized configuration of the MCHT exhibits such a half plume angle experimentally.

(5) The possible erosion of the annular channel has finally been studied, the energy of the ions impacting on the walls of the annular part is low enough not to cause erosion.

Acknowledgements

The two-dimensional model development has been performed in the frame of the Groupement De Recherche CNRS/CNES/SNECMA/Universités n°2759 "Propulsion Spatiale à Plasma".

References

[1]Khayms, V., and Martinez-Sanchez, M., "Fifty-Watt Hall Thruster for Microsatellites", *Micropropulsion for Small Spacecraft*, edited by M. M. Micci and A. D. Ketsdever, Progress in Astronautics and Aeronautics, AIAA, Washington, DC, 2000, Vol. 187, Chap. 9, pp. 233-254.

[2]Jacobson, D., and Jankovsky, R., "Test Results of a 200 W Class Hall Thruster", *34th Joint Propulsion Conference and Exhibit*, Cleveland, OH, paper AIAA-98-3792.

[3]Raitses, Y., and Fisch, N. J., "Parametric Investigation of a Nonconventional Hall Thruster", *Phys. Plasmas*, Vol. 8, No. 5, 2001, pp. 2579-2586.

[4]Smirnov, A., Raitses Y., and Fisch, N. J., "Electron Cross-Field Transport in a Miniaturized Cylindrical Hall Thruster", *IEEE Trans. Plasma Science,* Vol. 8, No. 2, 2006, pp. 132-141.

[5]Shirasaki, A., and Tahara, H., "Operational Characteristics and Plasma Measurements in Cylindrical Hall Thrusters", *J. Appl. Phys.,* Vol. 101, 2007, 073307.

[6]Smirnov, A., Raitses, Y., and Fisch, N. J., "Parametric Investigation of Miniaturized Cylindrical and Annular Hall Thrusters", *J. Appl. Phys.,* Vol. 92, No. 6, 2002, pp. 5673-5679.

[7]Smirnov, A., Raitses, Y., and Fisch, N. J., "Plasma Measurements in a 100 W Cylindrical Hall Thrusters", *J. Appl. Phys.,* Vol. 95, No. 5, 2004, pp. 2283-2292.

[8]Raitses, Y., Smirnov, A., and Fisch, N. J., "Enhance Performance of Cylindrical Hall Thrusters", *Appl. Phys. Lett. ,* Vol. 90, 2007, 221502.

[9]Smirnov, A., Raitses, Y., and Fisch, N. J., "Electron Cross-Field Transport in a Low Power Cylindrical Hall Thruster", *Phys. Plasmas,* Vol. 11, No. 11, 2004, pp. 4922-4933.

[10]Hagelaar, G. J. M., Bareilles, J., Garrigues, L., and Boeuf, J. P., "Two Dimensional Model of a Stationary Plasma Thruster", *J. Appl. Phys.*, Vol. 91, No. 9, 2002, pp. 5592-5598.

[11]Perez-Luna, J., Hagelaar, G. J. M., Garrigues, L., and Boeuf, J. P., "Model Analysis of a Double Stage Hall Effect Thruster with Double-Peaked Magnetic Field and Intermediate Electrode", *30th International Electric Propulsion Conference,* Florence, Italy September 17-20, 2007..

[12]Hagelaar, G. J. M., "Modelling Electron Transport in Magnetized Low Temperature Discharge Plasmas", *Plasma Sources Sci. Technol.*, Vol. 16, 2007, pp. S57-S66.

[13]Domonkos, M., "A Particle and Energy Balance Model of the Orificed Hollow Cathode ", *38th Joint Propulsion Conference and Exhibit*, Indianapolis, IN, paper AIAA-2002-4240.

[14]Garrigues, L., Hagelaar, G. J. M., Bareilles, J., Boniface, C., and Boeuf, J. P., "Model Study of the Influence of the Magnetic Field Configuration and a Performance and Lifetime of a Hall Thruster", *Phys. Plasmas,* Vol. 10, No. 12, 2003, pp. 4886-4892.

[15]Kaufman, H. R., Robinson, R. S., Seddon, R. I., "End-Hall Ion Source", *J. Vac. Sci. Technol. A*, Vol. 5, No. 4, 1987, pp. 2081-2084.

[16]Lieberman, M. A., and Lichtenberg, A. J., *Principles of Plasma Discharges and Materials Processing,* 2nd ed., Wiley, Hoboken, 1994, Chap. 5.

[17]Keidar, M., and Boyd, I. D., "On the Magnetic Mirror Effect in Hall Thrusters", *Appl. Phys. Lett.,* Vol. 87, 2005, 121501.

[18]Puech, V., and Mizzi, S., "Collision Cross Sections and Transport Parameters in Neon and Xenon", *J. Phys. D: Appl. Phys.*, Vol. 24, No. 11, 1991, pp. 1974-1985.

[19]Wetzel, R. C., Baiocchi, F. ., Hayes, T. R., and Freund, R. S., "Absolute Cross Sections for Electron-Impact Ionization of the Rare-Gas Atoms by Fast-Neutral-Beam Method", *Phys. Rev. A*, Vol. 35, No. 2, 1987, pp. 559-577.

[20]Achenbach, C., Muller, A., Salzborn, E., and Becker, R., "Single Ionization of Multiply Charged Xenon Ions by Electron Impact", *J. Phys. B: At. Mol. Phys.*, Vol. 17, 1984, No. 7, pp. 1405-1425.

[21]Boniface, C., Garrigues, L., Hagelaar, G. J. M., Boeuf, J. P., Gawron, D., and Mazouffre S., "Anomalous Cross Field Electron Transport in a Hall Effect Thruster", *Appl. Phys. Lett.*, Vol. 89, 2006, 161503.

[22]Bareilles, J., Hagelaar, G. J. M., Garrigues, L., Boniface, C., Boeuf, J. P., and Gascon, N., "Critical Assessment of a Two Dimensional Hybrid Hall Thruster Model : Comparisons with Experiments", *Phys. Plasmas,* Vol. 11, No. 6, 2004, pp. 3035-3046.

[23]Raitses, Y., Smirnov, A., Granstedt, E., Fisch N. J., "Overrun Discharge Current Operation of Low Power Cylindrical Hall Thrusters", IEPC 2007-222, *30th International Electric Propulsion Conference*, Florence, Italy September 17-20, 2007.